






**Thermodynamic and electronic properties of ReN<sub>2</sub> polymorphs at high pressure**


Ferenc Tasnádi <sup>1</sup>, Florian Bock <sup>1</sup>, Alena V. Ponomareva <sup>2</sup>, Maxim Bykov <sup>3</sup>, Saiana Khandarkhaeva,<sup>3,4</sup>  
Leonid Dubrovinsky,<sup>3</sup> and Igor A. Abrikosov <sup>1,2</sup>

<sup>1</sup>*Department of Physics, Chemistry, and Biology (IFM), Linköping University, SE-581 83 Linköping, Sweden*

<sup>2</sup>*Materials Modeling and Development Laboratory, NUST "MISIS," 119049 Moscow, Russia*

<sup>3</sup>*Bayerisches Geoinstitut, University of Bayreuth, D-95440 Bayreuth, Germany*

<sup>4</sup>*Material Physics and Technology at Extreme Conditions, Laboratory of Crystallography, University of Bayreuth, Universitätsstrasse 30, D-95440 Bayreuth, Germany*

 (Received 9 July 2021; revised 21 September 2021; accepted 18 October 2021; published 8 November 2021)

The high-pressure synthesis of rhenium nitride pernitride with a crystal structure that is unusual for transition metal dinitrides and high values of hardness and bulk modulus attracted significant attention to this system. We investigate the thermodynamic and electronic properties of the  $P2_1/c$  phase of ReN<sub>2</sub> and compare them with two other polytypes, the  $C2/m$  and  $P4/mbm$  phases, suggested in the literature. Our calculations of the formation enthalpy at zero temperature show that the former phase is the most stable of the three up to a pressure  $p = 170$  GPa, followed by the stabilization of the  $P4/mbm$  phase at higher pressure. The theoretical prediction is confirmed by diamond anvil cell synthesis of the  $P4/mbm$  ReN<sub>2</sub> at  $\approx 175$  GPa. Considering the effects of finite temperature in the quasiharmonic approximation at  $p = 100$  GPa we demonstrate that the  $P2_1/c$  phase has the lowest free energy of formation at least up to 1000 K. Our analysis of the pressure dependence of the electronic structure of rhenium nitride pernitride shows the presence of two electronic topological transitions around 18 GPa, when the Fermi surface changes its topology due to the appearance of an electron pocket at the high-symmetry  $Y_2$  point of the Brillouin zone while the disruption of the neck takes place slightly off from the  $\Gamma$ - $A$  line.

DOI: [10.1103/PhysRevB.104.184103](https://doi.org/10.1103/PhysRevB.104.184103)

**I. INTRODUCTION**

The high-pressure diamond anvil cell (DAC) experiment is a successful approach to establish a wide variety of physical conditions for synthesizing materials [1–3]. However, exploring metastable phases of materials is a challenging experimental task because one has to achieve control of the small free-energy barriers separating different polymorphs. On the other hand, computational high-throughput approaches [4,5] with sophisticated structure prediction algorithms [6,7] have entered into the field to advance the materials discoveries. The launch of the Materials Genome Initiative (MGI) [8] has further accelerated this trend [9,10] and triggered the need to develop an infrastructure to store and utilize the data calculated for different materials. Large databases, such as NOMAD [11], Materials Project [12], AFLOW [13], BioExcel [14], Topological Material DataBase [15], etc., have been created, which contain different properties of both existing and hypothetical materials. Analyzing the data from the Materials Project database, Sun *et al.* observed that nitrides have the

largest thermodynamic scale of metastability, defined as the energy differences between stable and metastable structures,  $\approx 190$  meV/atom [16], making this class of materials very interesting for further experimental and theoretical exploration.

At the same time, DAC has been actively used to synthesize novel nitrogen-rich phases of transition metal nitrides [2,17]. One applies high pressure and temperature in a chamber filled with molecular nitrogen or azides (AN<sub>3</sub>, A = Li, Na, etc.) and metals, such as rhenium, tungsten, osmium, etc. [18,19]. The synthesized metastable and nitrogen-rich materials—polymeric forms of nitrogen chains have also been observed [17]—represent a class of high-energy-density materials often with superior mechanical properties [19].

One challenge of using the high-pressure experiment to discover novel materials with attractive properties is to quench them to ambient conditions. The work by Bykov *et al.* [19] has shown that the ReN<sub>2</sub> compound in the monoclinic  $P2_1/c$  phase discovered in a DAC experiment can be also synthesized in a larger amount in a large-volume press at lower pressure. This compound has a crystal structure that is unusual for transition metal dinitrides MN<sub>2</sub>. It contains covalently bound dinitrogen dumbbells and discrete nitrogen atoms and represents an example of a mixed nitride-pernitride compound. Quenched to ambient pressure, rhenium nitride pernitride showed high mechanical properties, a hardness of 36.7(8) GPa, and a very high value of the bulk moduli of 428(10) GPa. The  $P2_1/c$  phase was not reported in earlier experiments. Remarkably, despite numerous theoretical studies

Published by the American Physical Society under the terms of the [Creative Commons Attribution 4.0 International](https://creativecommons.org/licenses/by/4.0/) license. Further distribution of this work must maintain attribution to the author(s) and the published article's title, journal citation, and DOI. Funded by [Bibsam](https://www.bibsam.de/).

of the Re-N system at this composition, it was not predicted theoretically even with the use of advanced structure prediction algorithms.

Kawamura *et al.* [20] have reported the synthesis of ReN<sub>2</sub> at 7.7 GPa and 1473–1873 K, with a hexagonal  $P6_3/mmc$  (MoS<sub>2</sub> type) structure. Elastic and mechanical properties of the phase have been investigated using  $T = 0$  K density functional theory (DFT) calculations [21]. In the same year, Du *et al.* [22], based on DFT calculations, proposed the tetragonal  $P4/mmm$  phase of ReN<sub>2</sub> underlined by the existence of the same phase for ReB<sub>2</sub> [23]. However, static 0 K DFT calculations by Wang *et al.* [24] have ruled out the  $P4/mmm$  phase as the ground state of ReN<sub>2</sub>. Instead, the calculations have indicated that the monoclinic  $C2/m$  structure of ReN<sub>2</sub> is more stable at 0 K than the experimentally found  $P6_3/mmc$  phase. Furthermore, it has been shown that above 130 GPa the  $P4/mbm$  phase becomes the favored phase. A computational structural search for stable and metastable rhenium nitrides up to 100 GPa pressures has been conducted [25] using a sophisticated evolutionary algorithm implemented in USPEX [6]. The study has confirmed the  $C2/m$  phase of ReN<sub>2</sub> as the ground state between 10 and 100 GPa. The  $P4/mmm$ ,  $Pbcn$ , and  $P6_3/mmc$  phases have been found to be metastable in the investigated pressure range.

In the present paper we investigate the thermodynamic stability of the  $P2_1/c$  phase with respect to the competing tetragonal  $P4/mbm$  and  $C2/m$  monoclinic phases in the pressure range between 0 and 180 GPa. We use first-principles electronic structure calculations and a quasiharmonic approximation for the lattice dynamics and establish that the former is indeed thermodynamically more stable than the two other polymorphs at pressures up to  $\approx 170$  GPa. At higher pressures the calculations predict the stabilization of the  $P4/mbm$  phase. As this phase was not reported in earlier experiments, we carry out the high-pressure synthesis of ReN<sub>2</sub> in a diamond anvil cell at  $\approx 175$  GPa. The theoretical prediction is verified by a characterization of the synthesized sample, which confirms the stabilization of the  $P4/mbm$  ReN<sub>2</sub>. Moreover, we calculate electronic properties of the  $P2_1/c$  phase and show the presence of two electronic topological transitions at  $\approx 18$  GPa.

## II. COMPUTATIONAL DETAILS

Simulations of the phase stability at  $T = 0$  K have been performed using the QUANTUM ESPRESSO (QE) program package [26] with projector augmented-wave (PAW) pseudopotentials [27] using 60 Ry for the kinetic energy cutoff and 350 Ry for the density and potential cutoff. The exchange correlation energy was approximated by the Perdew-Burke-Ernzerhof generalized gradient functional (PBE-GGA) [28]. In the case of the  $P4/mbm$  structure we have used a  $(16 \times 16 \times 23)$   $k$  mesh for sampling the Brillouin zone and the equation of state has been derived through fitting of the calculated total energies at different volumes by the third-order Burch-Murnighan expression. The two monoclinic structures ( $C2/m$  and  $P2_1/c$ ) have been relaxed by applying the variable cell shape method introduced by Wentzcovitch [29] using a  $(18 \times 10 \times 14)$  sampling of the Brillouin zone. The density of states has been calculated after doubling the  $k$ -mesh

TABLE I. The size of the structural models and the applied sampling of the Brillouin zone to calculate formation enthalpy and the phonon dispersions.

| Structure                 | Supercell               | $k$ -point mesh            | Supercell               | $k$ -point mesh         |
|---------------------------|-------------------------|----------------------------|-------------------------|-------------------------|
| cg-N                      | $(1 \times 1 \times 1)$ | $(23 \times 23 \times 23)$ | $(4 \times 4 \times 4)$ | $(5 \times 5 \times 5)$ |
| hcp Re                    | $(1 \times 1 \times 1)$ | $(15 \times 15 \times 10)$ | $(5 \times 5 \times 4)$ | $(5 \times 5 \times 5)$ |
| $P4/mbm$ ReN <sub>2</sub> | $(1 \times 1 \times 1)$ | $(19 \times 19 \times 27)$ | $(3 \times 3 \times 5)$ | $(5 \times 5 \times 5)$ |
| $C2/m$ ReN <sub>2</sub>   | $(1 \times 1 \times 1)$ | $(9 \times 21 \times 7)$   | $(4 \times 4 \times 2)$ | $(5 \times 5 \times 5)$ |
| $P2_1/c$ ReN <sub>2</sub> | $(1 \times 1 \times 1)$ | $(24 \times 14 \times 18)$ | $(3 \times 2 \times 3)$ | $(3 \times 3 \times 3)$ |

density. Fermi surfaces have been calculated and visualized using XCRYSDEN [30] and VESTA [31].

The free energies of formation have been calculated within the quasiharmonic approximation using PHONOPY [32] combined with force calculations performed with VASP [33–36]. In all VASP calculations the energy cutoff was set to 700 eV. Table I lists the supercell sizes and the applied sampling of the Brillouin zone in the VASP calculations. To underline the agreement of our simulations by QE and VASP, we have compared the stress tensor elements of the three different phases at around 100 GPa with unrelaxed atomic positions in the unit cells using the supercell sizes and  $k$ -point samplings from Table I. The deviations are less than 4 GPa. The largest error, 4%, has been observed for  $\sigma_{yy}$  in the case of comparing the  $P2_1/c$  and  $C2/m$  phases. In the enthalpy calculations the hcp phase of rhenium [37] and the cubic gauche phase of nitrogen (which is stable up to  $\approx 150$  GPa) have been used as the end-member states [38].

## III. EXPERIMENTS

A piece of Re metal was placed in a sample chamber of a BX90 diamond anvil cell [39] equipped with Boehler-Almax type diamonds (40- $\mu$ m culet diameters). Nitrogen served as a pressure-transmitting medium and as a reagent [40]. The DAC was compressed up to a target pressure of  $\approx 175$  GPa and laser heated using double-sided laser-heating systems installed at the Bayerisches Geoinstitute (BGI, Bayreuth, Germany) [41]. The sample was studied by means of powder and single-crystal x-ray diffraction at the synchrotron beamline ID11 of the ESRF using a monochromatic x-ray beam focused to  $\approx 0.3 \times 0.3 \mu\text{m}^2$ . For the single-crystal XRD measurements the sample was rotated around the vertical  $\omega$  axis in a range  $\pm 38^\circ$ . The diffraction images were collected with an angular step  $\Delta\omega = 0.5^\circ$  and an exposure time of 10 s/frame. For analysis of the single-crystal diffraction data (indexing, data integration, frame scaling, and absorption correction) we used the CRYCALISPRO software package. To calibrate an instrumental model in the CRYCALISPRO software, i.e., the sample-to-detector distance, detector origin, offsets of goniometer angles, and rotation of both the x-ray beam and the detector around the instrument axis, we used a single crystal of orthoenstatite ( $\text{Mg}_{1.93}\text{Fe}_{0.06}$ )( $\text{Si}_{1.93}, \text{Al}_{0.06}$ )O<sub>6</sub>,  $Pbca$  space group,  $a = 8.8117(2)$ ,  $b = 5.18320(10)$ , and  $c = 18.2391(3)$  Å. The structure was solved based on the single-crystal XRD data using the SHELXT structure solution program [42] by intrinsic phasing and refined using the OLEX2 program [43]. Pressure was determined based on the equation of state of

TABLE II. Space group numbers and the lattice parameters of the investigated  $\text{ReN}_2$  phases at  $T = 0$  K and  $p = 0$  GPa.

| Structure | Space group      | Lattice parameters ( $\text{\AA}$ )                      |
|-----------|------------------|--|
| $P2_1/c$  | 14 (monoclinic)  | $a = 3.630, b = 6.432, c = 4.977, \beta = 111.511^\circ$ |
| $C2_m$    | 12 (monoclinic)  | $a = 6.800, b = 2.824, c = 9.336, \beta = 142.35^\circ$  |
| $P4/mbm$  | 127 (tetragonal) | $a = b = 4.376, c = 2.650$                               |

Re. The refined unit cell volume of Re,  $22.50(4)$   $\text{\AA}^3$ , may correspond to pressures of 172.5 GPa [37], 177 GPa [44], or even 206 GPa [45].

#### IV. RESULTS

Figure 1 shows three polymorphs of  $\text{ReN}_2$  considered in this study:  $P2_1/c$ ,  $C2/m$ , and  $P4/mbm$ . The large sized spheres represent the rhenium atoms, while the small ones the nitrogen atoms or dumbbells. The discrete nitrogen atoms are denoted by  $N_1$ . If a nitrogen atom binds to another one and they form a dumbbell, then both nitrogen atoms are labeled by  $N_2$ . The  $P4/mbm$  structure contains only nitrogen dumbbells, while the two monoclinic structures have both types of nitrogen. Table II summarizes the optimized structural parameters obtained at  $T = 0$  K and  $p = 0$  GPa.

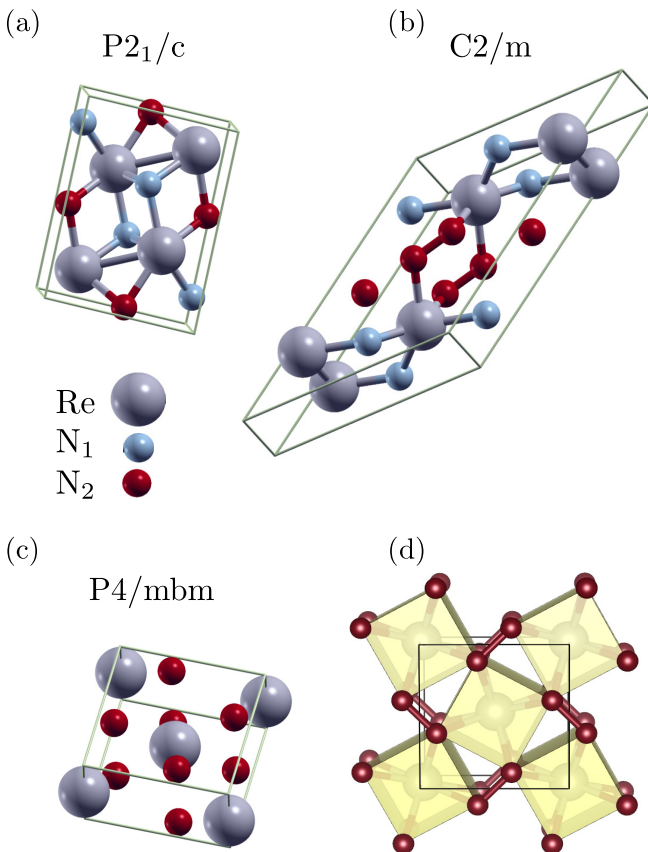


FIG. 1. The  $P2_1/c$ ,  $C2/m$ , and  $P4/mbm$  phases of  $\text{ReN}_2$ . Big circles show the Re atoms, while the small ones the nitrogen singles ( $N_1$ ) and dumbbells ( $N_2$ ). (d) shows the structure of the  $P4/mbm$  structure and the formed  $\text{ReN}_8$  rectangular prisms at  $\approx 175$   $\text{\AA}$  GPa as seen along the  $c$  axis.

In Fig. 2(a) we present the calculated formation enthalpy differences ( $\Delta H$ ) for the  $P2_1/c$  and  $P4/mbm$  phases in the pressure interval from 0 to 180 GPa relative to the values obtained for the  $C2/m$  phase. The relevance of spin-orbit coupling (SOC) effects on the formation energy differences between the  $P2_1/c$  and  $C2/m$  phases at 0 GPa can be ruled out by the electronic band structures calculated without SOC—see Materials Project [12] IDs mp-1077354 and mp-1019055.

The figure shows that the recently synthesized  $P2_1/c$  phase is the most stable of the three up to  $\approx 170$  GPa at  $T = 0$  K. Above this pressure the tetragonal phase is favored over the two monoclinic structures. Another interesting observation is that the  $P2_1/c$  phase is favored over the  $C2/m$  monoclinic phase in the whole pressure range. The dynamical stability at 0 GPa has been proven for all three phases earlier [19,25,46]. The effect of temperature on the relative stability of the three phases is analyzed in Fig. 2(b). The figure shows the Gibbs free energy of formation of the  $P2_1/c$ ,  $C2/m$ , and  $P4/mbm$

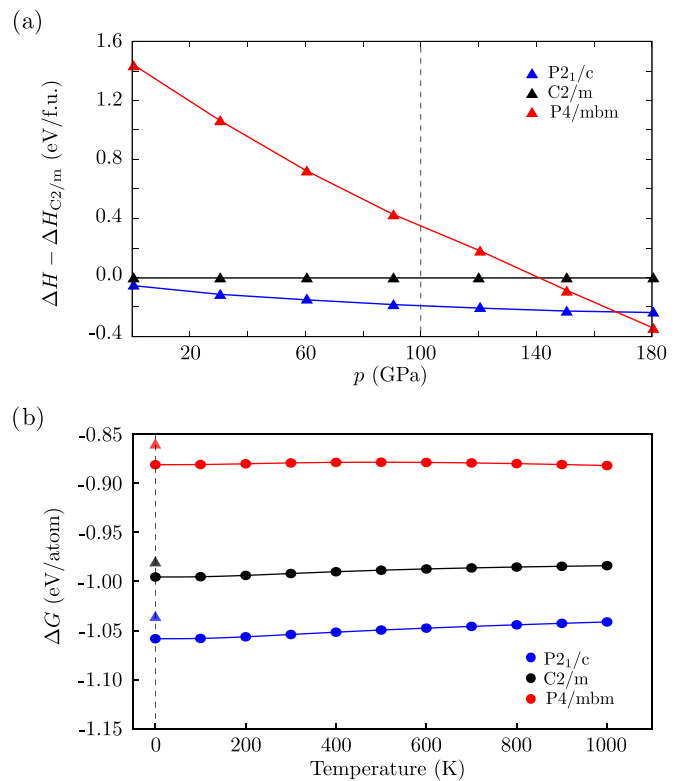


FIG. 2. (a) Formation enthalpy differences of the  $P2_1/c$ ,  $C2/m$ , and  $P4/mbm$  phases of  $\text{ReN}_2$  with respect to the  $C2/m$  phase. (b) Gibbs free energy of formation of the  $P2_1/c$ ,  $C2/m$ , and  $P4/mbm$  phases at 100 GPa within the quasiharmonic approximation up to 1000 K. The dashed vertical line is used to make a correspondence between (a) and (b)—see text.

TABLE III. Data collection, refinement, and crystal structure data for the  $P4/mbm$  polymorph of  $\text{ReN}_2$ .

| Crystal data  |  |
|---|--|
| Chemical formula  | $\text{ReN}_2$   |
| $M_r$   | 214.22   |
| Crystal system, space group   | Tetragonal, $P4/mbm$   |
| Pressure  | 175(10) GPa  |
| $a, c$ ( $\text{\AA}$ )   | 4.0013(12), 2.442(2)   |
| Volume  | 39.10(4)   |
| $Z$   | 2  |
| Radiation type  | Synchrotron, $\lambda = 0.3092 \text{\AA}$   |
| $\mu$ ( $\text{mm}^{-1}$ )  | 173.06   |
| Crystal size ( $\text{mm} \times \text{mm} \times \text{mm}$ )              | $0.001 \times 0.001 \times 0.001$  |
| Data collection   | ID11 ESRF  |
| Diffractometer  | Multiscan CRYSLIS PRO  |
| Absorption correction   | Empirical absorption correction using spherical harmonics implemented in SCALE3 ABSPACK scaling algorithm. |
| $T_{\min}, T_{\max}$  | 0.3165, 1.000  |
| No. of measured, independent, and observed [ $I > 2\sigma(I)$ ] reflections | 167, 59, 37  |
| $R_{\text{int}}$  | 0.060  |
| $(\sin \Theta / \lambda)_{\text{max}}$ ( $\text{\AA}^{-1}$ )                | 0.936  |
| Refinement  |  |
| $R[F^2 > 2\sigma(F^2)], wR(F^2), S$   | 0.043, 0.107, 1.02   |
| No. of reflections  | 59   |
| No. of parameters   | 6  |
| Crystal structure   |  |
| Wyckoff site  | Re, N  |
| Coordinates   | $2b, 4g$<br>$(0, 0, 0.5), [(0.618(9), 0.118(9), 0)]$   |

phases at 100 GPa up to 1000 K. The dashed vertical line in Figs. 2(a) and 2(b) is used to establish the correspondence between the zero-temperature static calculations (triangles) and calculations including the effects of the lattice dynamics, e.g., the zero-point motion (circles). One sees that the relative order of the three phases is not changed by temperature, though the formation energy differences become slightly smaller with increasing temperature. In Fig. 2(b) along the dashed line the energy differences between the values marked by a triangle and a sphere shows the effect of the zero-point energies of the lattice vibrations for each of the phases.

The characterization of the high-pressure synthesized sample has shown that at  $\approx 175$  GPa  $\text{ReN}_2$  indeed crystallizes in the tetragonal space group ( $P4/mbm$ , No. 127) with Re and N occupying Wyckoff sites  $2b$  and  $4g$ , respectively. See Table III and the Crystallographic Information File (CIF) in the Supplemental Material [47] for details. Figure 3 shows the x-ray reflections corresponding to the  $(hk\bar{2})$  reciprocal lattice plane of the  $P4/mbm$  phase. Re atoms are coordinated by eight nitrogen atoms forming  $\text{ReN}_8$  rectangular prisms. These prisms are stacked along the  $c$  axis (short edge of the rectangular prism) sharing faces and forming infinite columns. The columns also share common edges and additionally interconnected via N-N bonds as shown in Fig. 1(d). The refined N-N distance of  $1.34 \text{\AA}$  is close to the expected value of a single N-N bond at this pressure [48], suggesting that nitrogen forms a pernitride anion  $[\text{N-N}]^{4-}$ , while Re has an oxidation state +4.

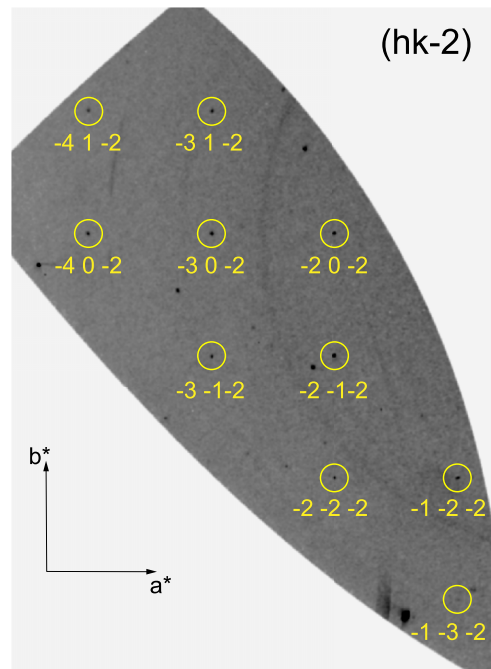


FIG. 3. Reconstructed precession images showing the  $(hk\bar{2})$  reciprocal lattice plane of  $P4/mbm$   $\text{ReN}_2$  at  $\approx 175$  GPa. The indexed reflections are encircled. Nonindexed reflections correspond to other grains of  $\text{ReN}_2$ , which are present in the sample.

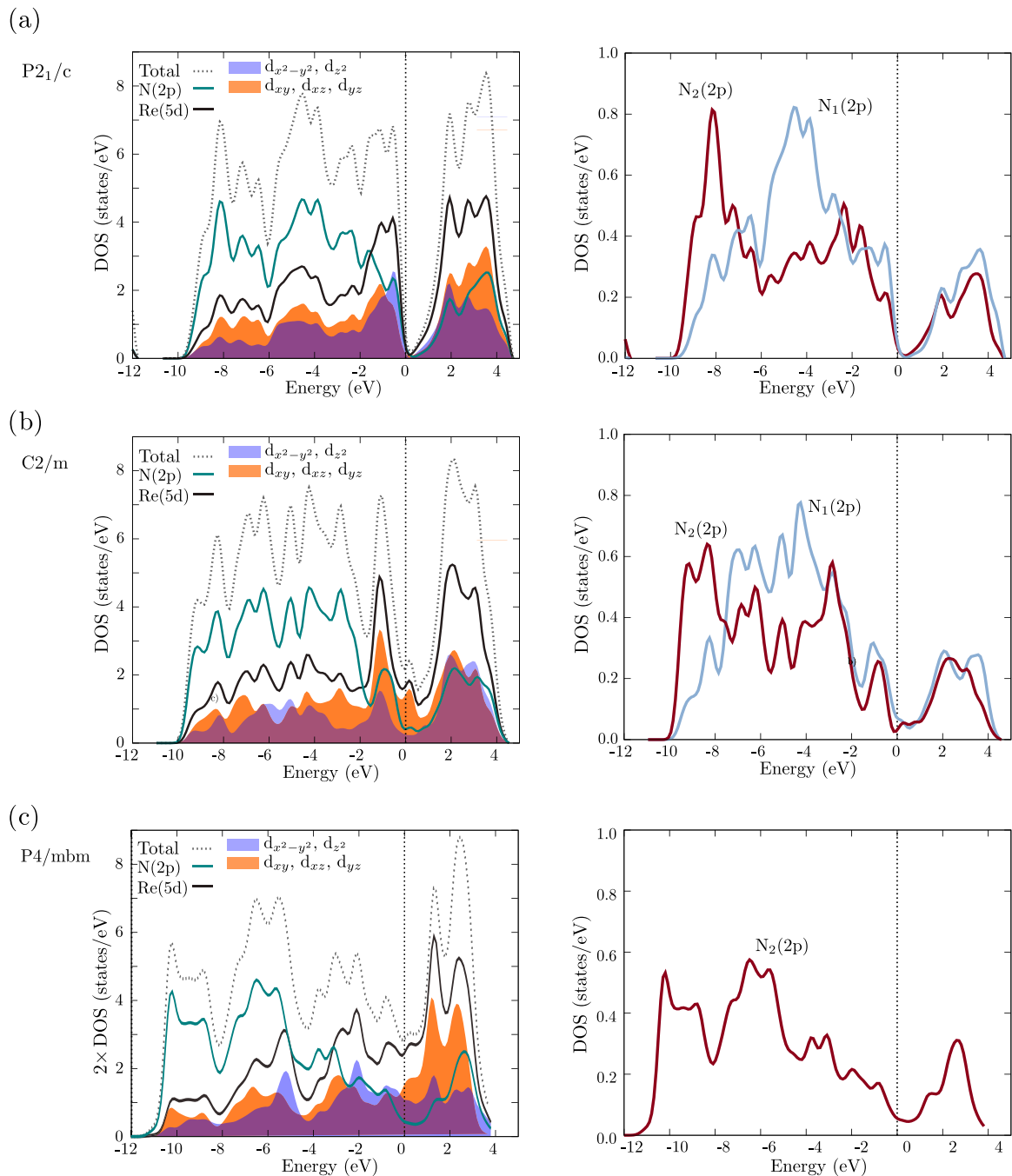


FIG. 4. Calculated total and partial density of states in (a)  $P2_1/c$ , (b)  $C2/m$ , and (c)  $P4/mbm$  phases of  $\text{ReN}_2$  at 0 GPa and  $T = 0$  K.

To understand the electronic properties of  $\text{ReN}_2$  polymorphs at 0 GPa we have calculated the electronic structure of all three phases. The calculated total and partial density of states (DOS) are shown in Figs. 4(a)–4(c). For each phase the first panel shows the total DOS curves including the total rhenium 5d partial DOS as shaded curves. One should note here that the tetragonal polymorph has half as many atoms as the other two, therefore double the DOS is plotted. The second panel compares the nitrogen 2p partial DOS for the different types ( $N_1$  and  $N_2$ ) nitrogens. In comparison, the total DOS of the three structures show different characteristics at the Fermi level. One observes nearly semimetallic behavior for

$P2_1/c$  and significantly more typical metallic behavior for the two competing phases. For the  $P2_1/c$  phase the calculations predict a low DOS value at the Fermi energy. In the case of  $C2/m$ , one sees instead a peak close to the Fermi energy, though the Fermi level is located in a valley between the two peaks. This could indicate a smaller contribution from the one-electron energy to the structural stability of the  $C2/m$  phase relative to the  $P2_1/c$  phase. In comparison, for  $P4/mbm$  one observes a finite value of the total DOS with a plateau in a vicinity of the Fermi energy. It also indicates a smaller contribution from the one-electron term to the structural stability of the phase. For each of the polymorphs, one notes significant

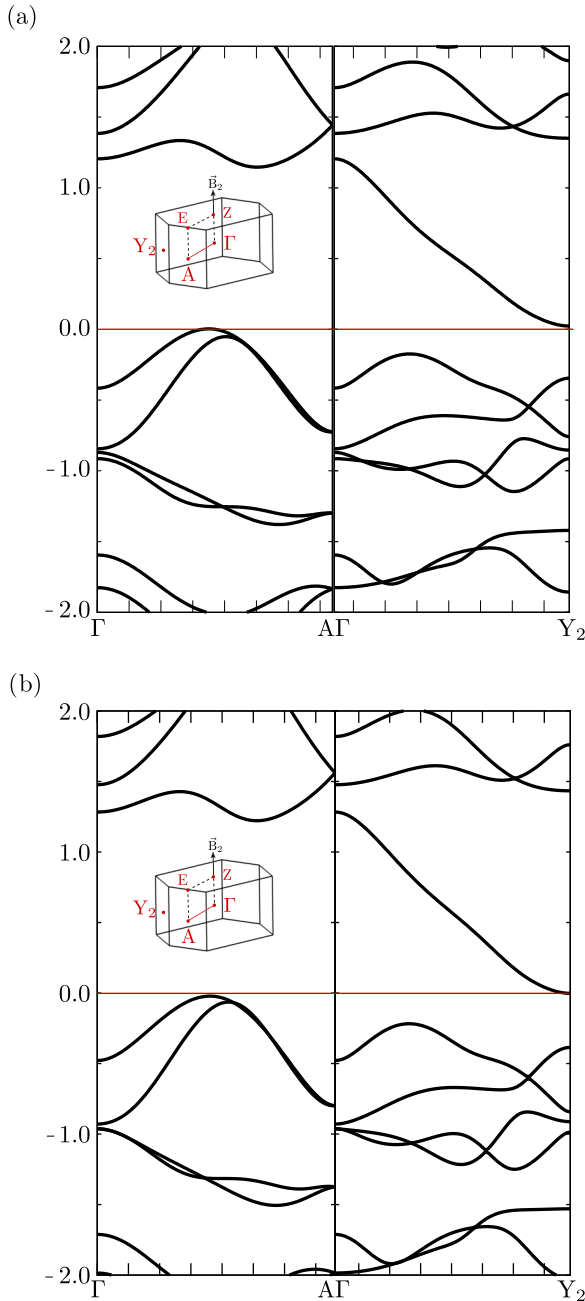


FIG. 5. Electronic band structure of  $P2_1/c$   $\text{ReN}_2$  at (a)  $p = 0$  GPa and (b) 23 GPa. The lines show the electronic bands parallel to the  $\Gamma$ - $A$  and  $\Gamma$ - $Y_2$  paths in the Brillouin zone.

hybridization between the Re  $5d$  and N  $2p$  orbitals. However, the strongly distorted trigonal prismatic local environments of the Re atoms do not allow any deeper analysis of the Re  $5d$  orbitals using crystal field theory.

To analyze the nearly semimetallic DOS of the  $P2_1/c$  phase we have calculated the electronic band structure in the Brillouin zone parallel to the  $\Gamma$ - $A$  and  $\Gamma$ - $Y_2$  paths (see the inset figure of the Brillouin zone in Fig. 5). Figure 5(a) shows the band structures at ambient pressure while Fig. 5(b) shows it for 23 GPa. One observes that the unoccupied band at  $Y_2$  and the occupied band along the  $\Gamma$ - $A$  line could be responsible for the semimetallic behavior at  $p = 0$  GPa. However, there

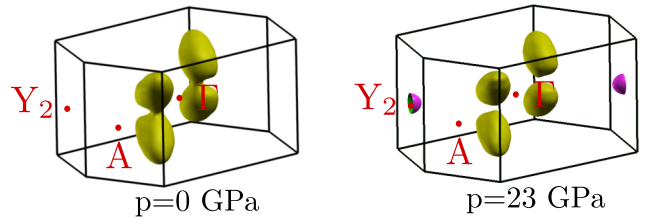


FIG. 6. Fermi surfaces of the  $P2_1/c$  phase of  $\text{ReN}_2$  at 0 and 23 GPa.

are small electron pockets along the lines in the  $\Gamma$ - $A$ - $E$ - $Z$  plane (not shown) which are responsible for the finite DOS at the Fermi energy. Interestingly, with increasing pressure [Fig. 5(b)] the band at  $Y_2$  passes the Fermi energy. Besides this, one sees that the band along the  $\Gamma$ - $A$  path crosses the Fermi energy, but not in the  $\Gamma$ - $A$ - $Y_2$  plane, where the valence band just touches the Fermi energy. Accordingly, one expects that the Fermi surface consists of a simple hole pocket around the  $\Gamma$ - $A$  line at low pressures, while at higher pressure an additional electron pocket is expected around the  $Y_2$  point in the Brillouin zone. Thus, an electronic topological transition (ETT), that is the change of the Fermi surface topology [49], should be observed with increased pressure.

To investigate the topology of the Fermi surface and to calculate the pressure at which ETT occurs, we have increased the accuracy of the calculations by increasing the density of  $k$  points in the electronic structure calculations. We have selected the  $k$ -point sampling ( $26 \times 14 \times 20$ ) which provides sufficient resolution for the study of the ETT and its influence on the materials properties. Figure 6 shows the Fermi surface of the  $P2_1/c$  phase of  $\text{ReN}_2$  at 0 and 23 GPa. The figure underlines the appearance of the additional electron pocket around  $Y_2$  with increasing pressure. Importantly, one sees the second ETT associated with a disruption of the neck between the two sheets of the Fermi surface slightly off from the  $\Gamma$ - $A$  line. The ETT is connected to the band which touches the Fermi energy along this line at  $p = 0$  GPa (Fig. 6) and shifts below it with increasing pressure [Fig. 6(b)]. Based on the chosen 1 GPa pressure grid the calculations have shown that the two ETTs occur at  $18 \pm 0.5$  GPa.

Experimental identification of the pressure-induced ETT is a nontrivial task, as exemplified by the cases of Zn [50–53], Os [54–58], and Fe [59]. The point is that the thermodynamic potential and its first derivatives are not affected by an ETT, the second derivatives may show weak square-root shaped peculiarities, while strong peculiarities are observed only for the third derivatives of the thermodynamic potential, leading to a classification of ETTs as the so-called “ $2\frac{1}{2}$ ” order phase transitions. Indeed, Fig. 7 shows that, as expected, the pressure dependence of the lattice parameters ratios  $c/a$  and  $b/a$  obtained in highly converged calculations at  $T = 0$  K does not show any peculiarities. However, as pointed out in Ref. [59], the ETT should lead to peculiarities of the thermal expansion, and it can show up in the lattice parameter ratios measured at finite temperatures due to anisotropy of the thermal expansion. The effect was indeed observed experimentally in hcp Fe [59] and Os [58]. Interestingly, comparing the calculated zero-temperature lattice parameter ratios in Fig. 7 with the

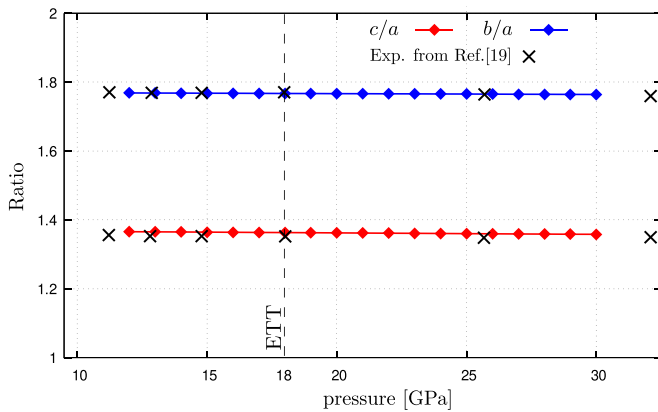


FIG. 7. Relative lattice parameters of the  $P2_1/c$  phase of  $\text{ReN}_2$  calculated with a  $k$  mesh of  $(26 \times 14 \times 20)$ .

room-temperature experiment of Ref. [19], we observe good agreement between the two data sets. But the experimental information at pressures around 18 GPa is, unfortunately, missing. Therefore, careful examination of the lattice parameters of the  $P2_1/c$  phase of  $\text{ReN}_2$  can be used to investigate the effect of the predicted ETT on the properties of this compound.

## V. CONCLUSIONS

We have investigated the thermodynamic and electronic properties of the  $P2_1/c$  phase of  $\text{ReN}_2$  in comparison with previously suggested, competing phases. Our density functional theory calculations at  $T = 0$  K have shown that the

$P2_1/c$  phase is the most stable polymorph of the three studied modifications of the compound up to  $\approx 170$  GPa. Above this pressure the tetragonal  $P4/mbm$  becomes more stable. This calculation is supported by the experiment. Using the quasiharmonic approximation we have shown that the  $P2_1/c$  phase is also a stable phase up to 1000 K at  $p = 100$  GPa. Moreover, our electronic structure calculations have shown that two nearly coexisting electronic topological transitions occur in the  $P2_1/c$  phase of  $\text{ReN}_2$  with increasing pressure. We propose additional experiments that should verify the theoretically predicted ETT.

## ACKNOWLEDGMENTS

We are grateful to Prof. M. I. Katsnelson for useful discussions. Support from the Knut and Alice Wallenberg Foundation (Wallenberg Scholar Grant No. KAW-2018.0194), the Swedish Government Strategic Research Areas in Materials Science on Functional Materials at Linköping University (Faculty Grant SFO-Mat-LiU No. 2009 00971) and SeRC, the Swedish Research Council (VR) Grant No. 2019-05600, and the VINN Excellence Center Functional Nanoscale Materials (FunMat-2) Grant No. 201605156 is gratefully acknowledged. Electronic structure calculations were supported by the Russian Science Foundation (Project No. 18-12-00492). The computations were enabled by resources provided by the Swedish National Infrastructure for Computing (SNIC) partially funded by the Swedish Research Council through Grant Agreement No. 2016-07213. The experiments were performed on beamline ID11 at the European Synchrotron Radiation Facility (ESRF), Grenoble, France. We are grateful to Pavel Sedmak at the ESRF for providing assistance in using the beamline.

- [1] P. F. McMillan, *Nat. Mater.* **1**, 19 (2002).
- [2] M. Bykov, E. Bykova, G. Aprilis, K. Glazyrin, E. Koemets, I. Chuvashova, I. Kuppenko, C. McCammon, M. Mezouar, V. Prakapenka, H.-P. Liermann, F. Tasnádi, A. V. Ponomareva, I. A. Abrikosov, N. Dubrovinskaia, and L. Dubrovinsky, *Nat. Commun.* **9**, 2756 (2018).
- [3] N. Dubrovinskaia, L. Dubrovinsky, N. A. Solopova, A. Abakumov, S. Turner, M. Hanfland, E. Bykova, M. Bykov, C. Prescher, V. B. Prakapenka, S. Petitgirard, I. Chuvashova, B. Gasharova, Y.-L. Mathis, P. Ershov, I. Snigireva, and A. Snigirev, *Sci. Adv.* **2**, e1600341 (2016).
- [4] A. Ludwig, *npj Comput. Mater.* **5**, 1 (2019).
- [5] K. Xia, H. Gao, C. Liu, J. Yuan, J. Sun, H.-T. Wang, and D. Xing, *Sci. Bull.* **63**, 817 (2018).
- [6] C. W. Glass, A. R. Oganov, and N. Hansen, *Comput. Phys. Commun.* **175**, 713 (2006).
- [7] C. J. Pickard and R. J. Needs, *J. Phys.: Condens. Matter* **23**, 053201 (2011).
- [8] J. J. de Pablo, N. E. Jackson, M. A. Webb, L.-Q. Chen, J. E. Moore, D. Morgan, R. Jacobs, T. Pollock, D. G. Schlom, E. S. Toberer, J. Analytis, I. Dabo, D. M. DeLongchamp, G. A. Fiete, G. M. Grason, G. Hautier, Y. Mo, K. Rajan, E. J. Reed, E. Rodriguez *et al.*, *npj Comput. Mater.* **5**, 1 (2019).
- [9] A. Agrawal and A. Choudhary, *APL Mater.* **4**, 053208 (2016).
- [10] W. Sun, A. Holder, B. Orvañanos, E. Arca, A. Zakutayev, S. Lany, and G. Ceder, *Chem. Mater.* **29**, 6936 (2017).
- [11] C. Draxl and M. Scheffler, *J. Phys. Mater.* **2**, 036001 (2019).
- [12] A. Jain, S. P. Ong, G. Hautier, W. Chen, W. D. Richards, S. Dacek, S. Cholia, D. Gunter, D. Skinner, G. Ceder, and K. A. Persson, *APL Mater.* **1**, 011002 (2013).
- [13] S. Curtarolo, W. Setyawan, G. L. W. Hart, M. Jahnatek, R. V. Chepulskii, R. H. Taylor, S. Wang, J. Xue, K. Yang, O. Levy, M. J. Mehl, H. T. Stokes, D. O. Demchenko, and D. Morgan, *Comput. Mater. Sci.* **58**, 218 (2012).
- [14] P. Andrio, A. Hospital, J. Conejero, L. Jordá, M. Del Pino, L. Codo, S. Soiland-Reyes, C. Goble, D. Lezzi, R. M. Badia, M. Orozco, and J. L. Gelpi, *Sci. Data* **6**, 169 (2019).
- [15] M. G. Vergniory, L. Elcoro, C. Felser, N. Regnault, B. A. Bernevig, and Z. Wang, *Nature (London)* **566**, 480 (2019).
- [16] W. Sun, S. T. Dacek, S. P. Ong, G. Hautier, A. Jain, W. D. Richards, A. C. Gamst, K. A. Persson, and G. Ceder, *Sci. Adv.* **2**, e1600225 (2016).
- [17] M. Bykov, E. Bykova, E. Koemets, T. Fedotenko, G. Aprilis, K. Glazyrin, H.-P. Liermann, A. V. Ponomareva, J. Tidholm, F. Tasnádi, I. A. Abrikosov, N. Dubrovinskaia, and L. Dubrovinsky, *Angew. Chem.* **57**, 9048 (2018).

- [18] M. Bykov, S. Chariton, E. Bykova, S. Khandarkhaeva, T. Fedotenko, A. V. Ponomareva, J. Tidholm, F. Tasnádi, I. A. Abrikosov, P. Sedmak, V. Prakapenka, M. Hanfland, H.-P. Liermann, M. Mahmood, A. F. Goncharov, N. Dubrovinskaia, and L. Dubrovinsky, *Angew. Chem.* **59**, 10321 (2020).
- [19] M. Bykov, S. Chariton, H. Fei, T. Fedotenko, G. Aprilis, A. V. Ponomareva, F. Tasnádi, I. A. Abrikosov, B. Merle, P. Feldner, S. Vogel, W. Schnick, V. B. Prakapenka, E. Greenberg, M. Hanfland, A. Pakhomova, H.-P. Liermann, T. Katsura, N. Dubrovinskaia, and L. Dubrovinsky, *Nat. Commun.* **10**, 2994 (2019).
- [20] F. Kawamura, H. Yusa, and T. Taniguchi, *Appl. Phys. Lett.* **100**, 251910 (2012).
- [21] I. R. Shein, A. N. Enyashin, and A. L. Ivanovskii, *Phys. Solid State* **55**, 1821 (2013).
- [22] X. P. Du, Y. X. Wang, and V. Lo, *Phys. Lett. A* **374**, 2569 (2010).
- [23] H.-Y. Chung, M. B. Weinberger, J. B. Levine, A. Kavner, J.-M. Yang, S. H. Tolbert, and R. B. Kaner, *Science* **316**, 436 (2007).
- [24] Y. Wang, T. Yao, J.-L. Yao, J. Zhang, and H. Gou, *Phys. Chem. Chem. Phys.* **15**, 183 (2013).
- [25] Z. Zhao, K. Bao, D. Li, D. Duan, F. Tian, X. Jin, C. Chen, X. Huang, B. Liu, and T. Cui, *Sci. Rep.* **4**, 4797 (2015).
- [26] P. Giannozzi, S. Baroni, N. Bonini, M. Calandra, R. Car, C. Cavazzoni, D. Ceresoli, G. L. Chiarotti, M. Cococcioni, I. Dabo, A. D. Corso, S. d. Gironcoli, S. Fabris, G. Fratesi, R. Gebauer, U. Gerstmann, C. Gougoussis, A. Kokalj, M. Lazzeri, L. Martin-Samos *et al.*, *J. Phys.: Condens. Matter* **21**, 395502 (2009).
- [27] P. E. Blöchl, *Phys. Rev. B* **50**, 17953 (1994).
- [28] J. P. Perdew, K. Burke, and M. Ernzerhof, *Phys. Rev. Lett.* **77**, 3865 (1996).
- [29] R. M. Wentzcovitch, J. L. Martins, and G. D. Price, *Phys. Rev. Lett.* **70**, 3947 (1993).
- [30] A. Kokalj, *J. Mol. Graphics* **17**, 176 (1999).
- [31] K. Momma and F. Izumi, *J. Appl. Crystallogr.* **44**, 1272 (2011).
- [32] A. Togo and I. Tanaka, *Scr. Mater.* **108**, 1 (2015).
- [33] G. Kresse and J. Hafner, *Phys. Rev. B* **47**, 558 (1993).
- [34] G. Kresse and J. Hafner, *Phys. Rev. B* **49**, 14251 (1994).
- [35] G. Kresse and J. Furthmüller, *Comput. Mater. Sci.* **6**, 15 (1996).
- [36] G. Kresse and J. Furthmüller, *Phys. Rev. B* **54**, 11169 (1996).
- [37] S. Anzellini, A. Dewaele, F. Occelli, P. Loubeyre, and M. Mezouar, *J. Appl. Phys.* **115**, 043511 (2014).
- [38] D. Laniel, B. Winkler, T. Fedotenko, A. Pakhomova, S. Chariton, V. Milman, V. Prakapenka, L. Dubrovinsky, and N. Dubrovinskaia, *Phys. Rev. Lett.* **124**, 216001 (2020).
- [39] I. Kantor, V. Prakapenka, A. Kantor, P. Dera, A. Kurnosov, S. Sinogeikin, N. Dubrovinskaia, and L. Dubrovinsky, *Rev. Sci. Instrum.* **83**, 125102 (2012).
- [40] A. Kurnosov, I. Kantor, T. Boffa-Ballaran, S. Lindhardt, L. Dubrovinsky, A. Kuznetsov, and B. H. Zehnder, *Rev. Sci. Instrum.* **79**, 045110 (2008).
- [41] T. Fedotenko, L. Dubrovinsky, G. Aprilis, E. Koemets, A. Snigirev, I. Snigireva, A. Barannikov, P. Ershov, F. Cova, M. Hanfland, and N. Dubrovinskaia, *Rev. Sci. Instrum.* **90**, 104501 (2019).
- [42] G. M. Sheldrick, *Acta Crystallogr., Sect. A* **71**, 3 (2015).
- [43] O. V. Dolomanov, L. J. Bourhis, R. J. Gildea, J. a. K. Howard, and H. Puschmann, *J. Appl. Crystallogr.* **42**, 339 (2009).
- [44] C.-S. Zha, W. A. Bassett, and S.-H. Shim, *Rev. Sci. Instrum.* **75**, 2409 (2004).
- [45] L. Dubrovinsky, N. Dubrovinskaia, V. B. Prakapenka, and A. M. Abakumov, *Nat. Commun.* **3**, 1163 (2012).
- [46] H. Yan, M. Zhang, Q. Wei, and P. Guo, *J. Alloy Compd.* **581**, 508 (2013).
- [47] See Supplemental Material at <http://link.aps.org/supplemental/10.1103/PhysRevB.104.184103> for the Crystallographic Information File (CIF) of ReN<sub>2</sub> in the *P4/mbm* tetragonal space group.
- [48] M. I. Eremets, A. G. Gavriluk, I. A. Trojan, D. A. Dzivenko, and R. Boehler, *Nat. Mater.* **3**, 558 (2004).
- [49] I. M. Lifshitz, *Sov. Phys. - JETP* **11**, 1130 (1960).
- [50] T. Kenichi, *Phys. Rev. B* **56**, 5170 (1997).
- [51] T. Kenichi, *Phys. Rev. B* **60**, 6171 (1999).
- [52] S. Klotz, M. Braden, and J. M. Besson, *Phys. Rev. Lett.* **81**, 1239 (1998).
- [53] G. Steinle-Neumann, L. Stixrude, and R. E. Cohen, *Phys. Rev. B* **63**, 054103 (2001).
- [54] T. Kenichi, *Phys. Rev. B* **70**, 012101 (2004).
- [55] F. Occelli, D. L. Farber, J. Badro, C. M. Aracne, D. M. Teter, M. Hanfland, B. Canny, and B. Couzinet, *Phys. Rev. Lett.* **93**, 095502 (2004).
- [56] M. M. Armentrout and A. Kavner, *J. Appl. Phys.* **107**, 093528 (2010).
- [57] B. K. Godwal, J. Yan, S. M. Clark, and R. Jeanloz, *J. Appl. Phys.* **111**, 112608 (2012).
- [58] L. Dubrovinsky, N. Dubrovinskaia, E. Bykova, M. Bykov, V. Prakapenka, C. Prescher, K. Glazyrin, H.-P. Liermann, M. Hanfland, M. Ekholm, Q. Feng, L. V. Pourovskii, M. I. Katsnelson, J. M. Wills, and I. A. Abrikosov, *Nature (London)* **525**, 226 (2015).
- [59] K. Glazyrin, L. V. Pourovskii, L. Dubrovinsky, O. Narygina, C. McCammon, B. Hewener, V. Schünemann, J. Wolny, K. Muffler, A. I. Chumakov, W. Crichton, M. Hanfland, V. B. Prakapenka, F. Tasnádi, M. Ekholm, M. Aichhorn, V. Vildosola, A. V. Ruban, M. I. Katsnelson, and I. A. Abrikosov, *Phys. Rev. Lett.* **110**, 117206 (2013).